HAL
open science

Dependence of the structural, transport and magnetic properties of Tl1-yFe2-z(Se1-xSx)2 with isovalent substitution of Se by S

Pierre Toulemonde, David Santos-Cottin, Christophe Lepoittevin, Pierre Strobel, Jacques Marcus

To cite this version:

Pierre Toulemonde, David Santos-Cottin, Christophe Lepoittevin, Pierre Strobel, Jacques Marcus. Dependence of the structural, transport and magnetic properties of Tl1-yFe2-z(Se1-xSx)2 with isovalent substitution of Se by S. Journal of Physics: Condensed Matter, 2013, 25, pp.075703. 10.1088/0953-8984/25/7/075703 . hal-00813599

HAL Id: hal-00813599

https://hal.science/hal-00813599v1

Submitted on 15 Apr 2013

HAL is a multi-disciplinary open access archive for the deposit and dissemination of scientific research documents, whether they are published or not. The documents may come from teaching and research institutions in France or abroad, or from public or private research centers.

L'archive ouverte pluridisciplinaire **HAL**, est destinée au dépôt et à la diffusion de documents scientifiques de niveau recherche, publiés ou non, émanant des établissements d'enseignement et de recherche français ou étrangers, des laboratoires publics ou privés.

Dependence of the structural, transport and magnetic properties of $Tl_{1-y}Fe_{2-z}(Se_{1-x}S_x)_2$ with isovalent substitution of Se by S

P. Toulemonde‡, D. Santos-Cottin§, Ch. Lepoittevin, P. Strobel and J. Marcus

Institut Néel, CNRS and Université Joseph Fourier, 25 avenue des Martyrs, BP 166, F-38042 Grenoble cedex 9, France.

E-mail: `pierre.toulemonde@grenoble.cnrs.fr`

Abstract.

The effect of selenium substitution by sulfur in the $Tl_{1-y}Fe_{2-z}Se_2$ antiferromagnet was studied by x-ray and electron diffraction, magnetization and transport measurements. $Tl_{0.8}Fe_{1.5}(Se_{1-x}S_x)_2$ (nominal composition) solid solution was synthesized in the full x range ($0 \leq x(S) \leq 1$) using the sealed tube technique. No superconductivity was found down to 4.2K in the series despite the fact that the optimal crystallographic parameters, determined by Rietveld refinements, are reached in the series (i.e. the Fe-(Se,S) interplane height and (Se,S)-Fe-(Se,S) angle for which the critical superconducting transition T_c is usually maximal in pnictides). Quasi full Tl site ($y \sim 0.05$) compared to significant alkaline deficiency ($y = 0.2 - 0.3$) in analogous $A_{1-y}Fe_{2-z}Se_2$ (A = K, Rb, Cs), and the resulting differences in iron valency, density of states and doping, are suggested to explain this absence of superconductivity. Transmission electron microscopy confirmed the existence of ordered iron vacancies network in the samples of the $Tl_{0.8}Fe_{1.5}(Se_{1-x}S_x)_2$ series in the form of the tetragonal $\sqrt{5}$ a $\times\sqrt{5}$ a $\times$ c superstructure ($I4/m$). The Néel temperature (T_N) indicating the onset of antiferromagnetism order in this $\sqrt{5}$ a $\times\sqrt{5}$ a $\times$ c supercell is found to decrease from 450K in the selenide (x=0) to 330K in the sulfide (x=1). We finally demonstrate a direct linear relationship between T_N and the Fe-(Se,S) bond length (or Fe-(Se,S) height).

PACS numbers: 74.70.Xa, 74.62.Bf, 61.05.cp, 75.50.Ee

‡ Corresponding author. Fax: 00334 7688 1038

§ Present address: IMPMC, Université Pierre et Marie Curie 4, place Jussieu, 75005 Paris, France

1. Introduction

After the discovery of superconductivity in iron-based superconductors, i.e. in pnictides and chalcogenides, numerous families were found, at least five families for arsenides with superconducting transition up to T_c = 55 K. In chalogenides, superconductivity was first found in the "11" family ($Fe_{1+y}(Te_{1-x}Ch_x)$) with Ch=Se or S, and recently in a second family $AFe_{2-y}Se_2$ ("A-122" selenide) with A=K [1], Rb, Cs (or Tl/Rb, Tl/Cs) showing T_c around 30 K, i.e. close to the maximum value measured for FeSe under high pressure [2, 3, 4]. A related compound is $TlFe_{2-y}Se_2$, which was first synthesized and studied 25 years ago by Häggström et al. [5]. This compound is antiferromagnetic with a high Néel temperature around T_N=450K, i.e. in the range of T_N values measured for alkaline intercalated 122 selenides [6].

In iron-based superconductors, superconductivity can be induced by simple isovalent substitution of the pnictogen or chalcogen, for example by substitution of As by P in LnFeAsO (Ln = La, Ce, Pr, Nd, Sm...) ("1111") or "122" arsenides, or of Te by Se/S in the $Fe_{1+y}Te$ telluride. The present work follows the same approach to search for superconductivity in thallium-122 selenide (" Tl-122") by substitution of selenium by sulfur. In addition, this substitution may allow to approach the structural conditions where the highest T_c's are reached in this structural family, i.e. either a Fe-Se bond length around 1.41 Å [7] (in the FeSe system under high pressure) or Ch-Fe-Ch bond angles corresponding to a regular $FeCh_4$ tetrahedron (in Fe-As systems) [8].

During this study we became aware of an investigation of the $K_{1-y}Fe_{2-z}(Se_{1-x}S_x)_2$ series by Lei et al. [9]. In the potassium system, the x = 0 end member is already superconducting (T_c = 33K) and superconductivity disappears with increasing x(S). This may be related to (i) a decrease in iron non-stoichiometry (i.e. the compound contains less iron vacancies), (ii) an increase in $FeCh_4$ tetrahedron distortion [9].

In this article we study the structural and physical trends vs. sulfur content in the $Tl_{1-y}Fe_{2-z}(Se_{1-x}S_x)_2$ series‖. Contrary to the alkaline-122 systems, the selenium-only and end-member is known to present no superconductivity. We will show in this article that all sulfur-substituted compositions remain antiferromagnetic above room temperature, and that their Néel temperature decreases linearly with decreasing Fe-Ch bond length.

‖ Members of the $Tl_{0.8}Fe_{1.5}(Se_{1-x}Te_x)_2$ (nominal composition) solid solution were also prepared up to x(Te) = 0.5 using the same synthesis technique. The preparation of phase-pure samples was more difficult : for $x > 0.2$ the samples contain secondary phases: tetragonal $Fe(Te_{1-x}Se_x)$, $FeTe_2$ and Tl_5Te_3. Tellurium substitution for selenium induces an increase in both a and c cell parameters (up to $a \sim 3.94$ $\AA$ and $c \sim 14.09$ $\AA$ for x(Te) = 0.5), as expected from the larger atomic radius of tellurium. Transport measurements in this system showed superconductivity (with zero resistivity) below T_c=15K. Magnetization measurements, however, gave a very small diamagnetic shielding, which can be ascribed to the tetragonal $Fe(Te_{1-x}Se_x)$ impurity, since the superconducting volume agrees with the $Fe(Te_{1-x}Se_x)$ phase fraction estimated from x-ray diffraction. We note that Te substitution in superconducting $Rb_{0.8}Fe_{2-y}(Se_{1-x}Te_x)_2$ induces a strong reduction of superconductivity which disappears for x(Te)=0.15 [10].

2. Experimental

$Tl_{1-y}Fe_{2-z}(Se_{1-x}S_x)_2$ samples ("Tl-122(Se,S)") were synthesized using the sealed tube technique as reported elsewhere for $Fe_{1+\delta}(Te_{1-x}Se_x)$ [11, 12]. Starting materials were commercial Fe pieces (Alfa Aesar, 99.98%), Tl pieces (Alfa Aesar, 99.99%), Se chips (Alfa Aesar, 99.999%) and FeS (Alfa Aesar, 99.9%). Precursors with nominal composition $Tl_{0.8}Fe_{1.5}(Se_{1-x}S_x)_2$ (i.e. z = 0.5) were placed in an alumina crucible which was introduced in a quartz tube and sealed under vacuum. The heat treatment constituted of a first heating ramp at 100 °C/h up to 700 °C followed by a plateau for 12 hours at this temperature; then the samples were slowly cooled at 5 °C/h to 280 °C and maintained at this temperature for 24h, then furnace-cooled.

X-ray diffraction (XRD) patterns were collected at room temperature using a Bruker D8 powder diffractometer working in Bragg-Brentano geometry at the wavelength $\lambda_{Cu,\ K\alpha 1} = 1.54056$ Å from $2\theta = 10$ to 90 ° with a step of 0.032 °.

Electron diffraction (ED) studies combined with quantitative energy dispersive spectroscopy (EDS) micro-analysis were carried out using a Philips CM 300 transmission electron microscope (TEM), operating at 300 kV, equipped with a +/- 30 ° double tilt sample holder. Specimens were prepared by crushing a small portion of sample in an agate mortar containing ethanol in order to obtain a powder with particles as thin as possible. Then a droplet of the mixture was deposited on a copper grid with a holey carbon film, in order to obtain an homogeneous particles distribution.

Transport measurements were carried out using the four point contacts technique down to liquid helium temperature. Magnetization of selected samples were measured at low (down to 4.2K) and high temperature (up to 600K) using a home-made magnetometer with a resolution of 2.10^{-6} A.m^2 and with magnetic field up to 6T.

3. Results and discussion

3.1. Powder x-ray diffraction

Figure 1 shows the powder x-ray diffraction (XRD) patterns of polycrystalline $Tl_{0.8}Fe_{1.5}(Se_{1-x}S_x)_2$ samples (nominal composition) for sulfur contents from 0 to 100% (with a step of substitution equal to 0.1). Nearly all peaks can be indexed in the tetragonal space group *I4/mmm* found for $AEFe_2As_2$ (AE = Ba, Sr, Ca) arsenides and used originally by Guo et al. [1] for their superconducting KFe_2Se_2 selenide. This *I4/mmm* tetragonal structure (drawn in the right part of fig. 3) implies disordered iron vacancies in the iron plane with an average iron occupancy factor around 0.8. Remaining unreacted (non superconducting) hexagonal $Fe(S_{1-x}Se_x)$ (marked by an asterisk symbol in fig.1) and Fe_3O_4 (for x(S)=0.8, symbol "+"in fig.1) are found as minor impurities in several samples. In addition we observe that a significant modification of the initial nominal composition Tl:Fe:Ch = 0.8:1.5:2 (for example an increase of iron content) induces the emergence of the tetragonal $Fe(Se_{1-x}S_x)$ secondary phase (XRD pattern not shown).

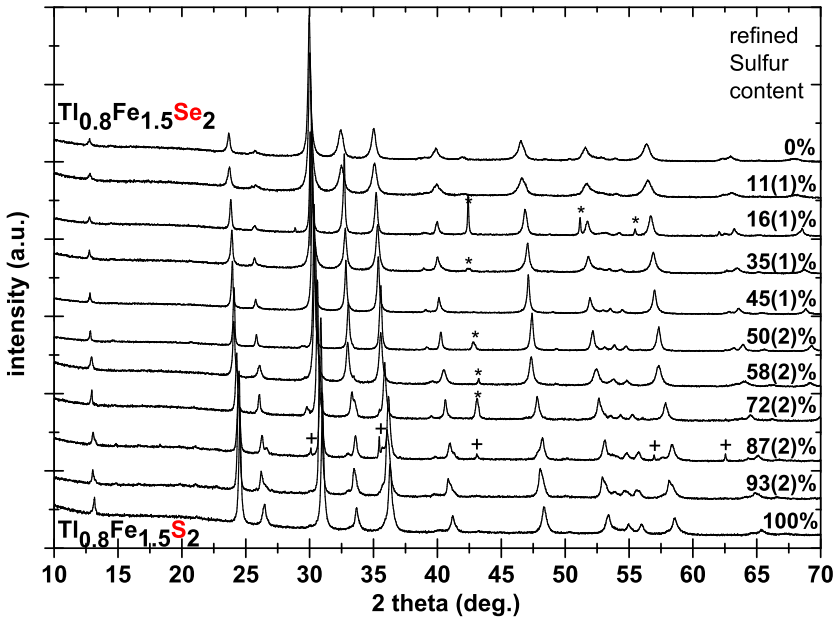

Figure 1. XRD patterns ($\lambda = 1.5406$ Å) of $Tl_{0.8}Fe_{1.5}(Se_{1-x}S_x)_2$ samples for $0 \leq x \leq 1$ (nominal step=0.1). Refined compositions (at. % S) are indicated. * and + symbols indicate the main Bragg peaks of (non superconducting) hexagonal $Fe(S_{1-x}Se_x)$ and Fe_3O_4 (for x=0.8) minor impurities respectively.

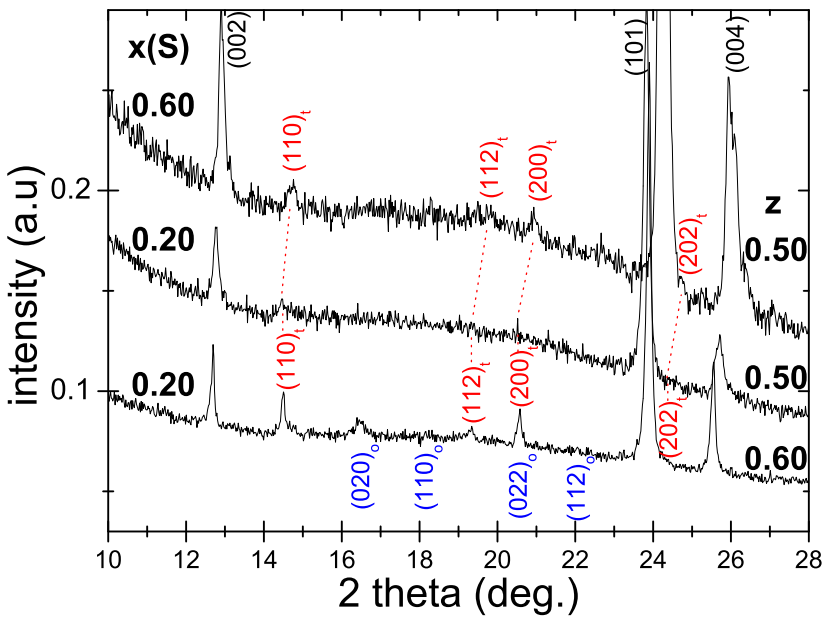

Figure 2. Selected low 2-theta region of the XRD patterns of x=0.2 (with z=0.5 or z=0.6) and x=0.6 $Tl_{0.8}Fe_{2-z}(Se_{1-x}S_x)_2$ samples ($\lambda = 1.5406$ Å). Supercell weak reflections related to the tetragonal $\sqrt{5}$ a $\times\sqrt{5}$ a $\times$ c (Miller indices labelled "t") or orthorhombic $\sqrt{2}$ a $\times 2\sqrt{2}$ a $\times$ c (labelled "o") superstructures are indicated.

More interesting, for some sulfur contents, we clearly observe very weak reflections (near the detection limit) at low angle. These supplementary Bragg peaks can be indexed in supercells derived from the original *I4/mmm* lattice. If a and c represent the subcell parameters, two superstructures were found in the present study: a tetragonal $\sqrt{5}$ a $\times$ $\sqrt{5}$ a $\times$ c one (*I4/m* space group) and an orthorhombic $\sqrt{2}$ a $\times$ $2\sqrt{2}$ a $\times$ c one (*Ibam*), only present if the iron deficiency is large. These superstructures are due to iron vacancy ordering observed for z=0.4 and z=0.5 by Sabrowsky et al. 25 years ago in $TlFe_{2-z}S_2$ sulfides [13], and confirmed very recently in the new alkaline-based selenides $AFe_{2-z}Se_2$ (A=K,Rb,Cs) [6, 14, 15, 16, 17] but also in the thallium-based one [18]. An enlargement of the low 2-theta region of the XRD patterns for $Tl_{0.8}Fe_{1.5}(Se_{0.4}S_{0.6})_2$, $Tl_{0.8}Fe_{1.5}(Se_{0.8}S_{0.2})_2$ (i.e. both with z=0.5) and $Tl_{0.8}Fe_{1.4}(Se_{0.8}S_{0.2})_2$ (i.e. z=0.6, not belonging to the series) is displayed figure 2. For x=0.6 (and z=0.5) the satellite peaks of the $\sqrt{5}$ a $\times$ $\sqrt{5}$ a $\times$ c supercell are clearly visible. For the sample with less sulfur, x=0.2 and the same nominal iron content (z=0.5) these satellite peaks are still present (the highest one being the (110) reflection)) but seem less intense. In contrast, when the level of iron vacancies is increased, i.e. for z=0.6 (keeping x=0.20), new small satellite peaks appear, in addition to those related to the $\sqrt{5}$ a $\times$ $\sqrt{5}$ a $\times$ c supercell, which can be indexed in the orthorhombic $\sqrt{2}$ a $\times$ $2\sqrt{2}$ a $\times$ c supercell. This result, confirmed by electron diffraction (see below), is in agreement with the previous work of Sabrowsky [13] who reported the orthorhombic supercell for low level of iron content in sulfides.

Despite the difficulty to detect the satellite reflections by conventional powder XRD, this XRD characterization suggests that all samples contain at least the $\sqrt{5}$ a $\times$ $\sqrt{5}$ a $\times$ c phase (mixed with the orthorhombic $\sqrt{2}$ a $\times$ $2\sqrt{2}$ a $\times$ c one if the nominal content of iron is decreased). To confirm this result we have performed an electron diffraction study of selected samples. In addition, because supercell reflections are extremely weak (near the detection level of our diffraction setup), all the Rietveld refinements of our XRD patterns were performed in the average *I4/mmm* space group.

An enlargement of two regions of the XRD patterns around (004) and (200) reflections of the Tl-122(Se,S) series shows a continuous shift to higher angle with sulfur content (Figure 3). This corresponds to a decrease of both lattice parameters of the Tl-122(Se,S) lattice with increasing x(S). The evolution of cell parameters and volume of the unit cell with sulfur content, determined from Rietveld refinement of XRD patterns are displayed respectively in figure 4. The decrease observed here (from a $\sim$ 3.88 Å and c $\sim$ 14 Å for x(S) = 0 to a $\sim$ 3.75 Å and c $\sim$ 13.4 Å for x(S) = 1, i.e. a reduction of the unit cell volume of about 10%, fig. 4(b)) is similar in amplitude to that reported in the potassium $K_{1-y}Fe_{2-z}(Se_{1-x}S_x)_2$ series (see fig. 1 in ref. [9]). The lines (guide for eyes) in fig. 4(a) show that our samples are in agreement with the expected values considering a linear decrease between extremal x = 0 and x = 100% compositions. The small deviation from this linear trend (visible in the c-axis variation for $x < 20\%$ for example) is probably due to very slight variations in iron and/or thallium contents between different samples (see the trend shown in table 1 for refined values of Fe and Tl site occupancy factors). About the real stoichiometry of the samples, as we will see

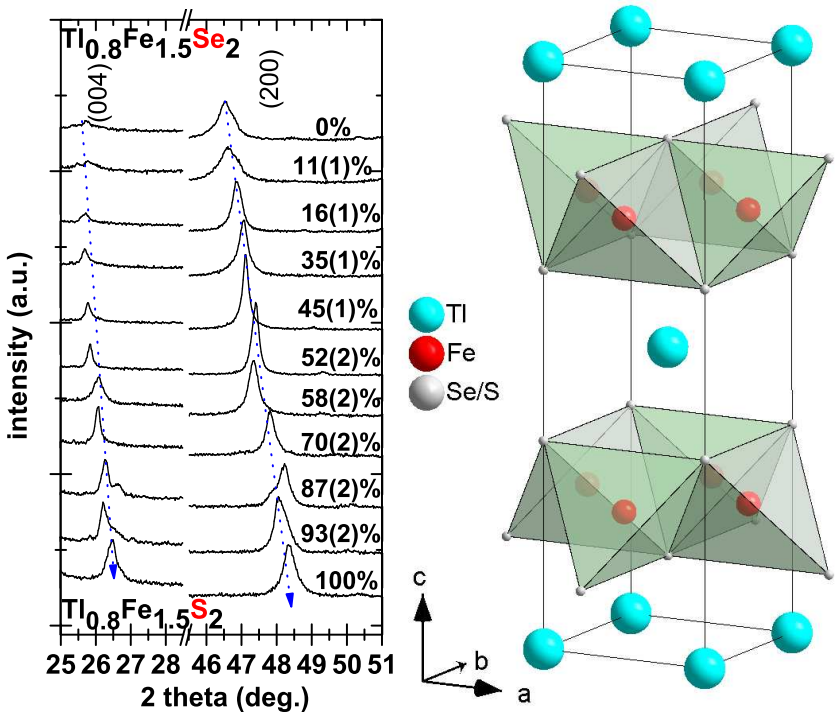

Figure 3. Left: Selected 2-theta regions of the XRD patterns in the $Tl_{0.8}Fe_{1.5}(Se_{1-x}S_x)_2$ series ($\lambda = 1.5406$ Å) showing the 2-theta shift of (004) and (200) reflections, corresponding to the shrinkage of the lattice with x(S) increase. Right: Tl-122(Se,S) structure in the *I4/mmm* space group (i.e. with iron vacancies not ordered).

it later in part D (Rietveld refinements results), we found that the Tl site is nearly full despite the fact that the nominal composition corresponds to 20% of deficiency (y = 0.2). This is an important difference with alkaline based A-122 selenides where real alkaline deficiency is generally around 20-30% in superconducting compounds [14, 17].

3.2. Electron diffraction in TEM

x=0, 0.2 (with z = 0.6, i.e. not belonging to our z = 0.5 series) and 0.7 compositions were selected for detailed electron diffraction studies.

For the pure selenide (x = 0, z = 0.5), the EDS analysis carried out on around 50 crystallites shows an homogeneous average cationic composition $Tl_{1.0(1)}Fe_{1.7(1)}Se_2$, in agreement with the Rietveld calculations (see paragraph 3.4) which evidences a significant amount of iron vacancies in the samples, as expected. The electron diffraction patterns recorded on different particles present a body-centered tetragonal sub-cell with a = b = 3.9 Å, c = 14 Å. The extinctions observed are compatible with the *I4/mmm* space group. However, extra reflections, i.e. satellite reflections, can be observed on the [001] oriented basal plane (figure 5). These extra spots are characteristic of a modulated structure with a two-components modulation vector $\vec{q^*} = \alpha\vec{a^*} + \beta\vec{b^*}$. According to this ED pattern, there are several ways to define the modulation vectors. We chose here

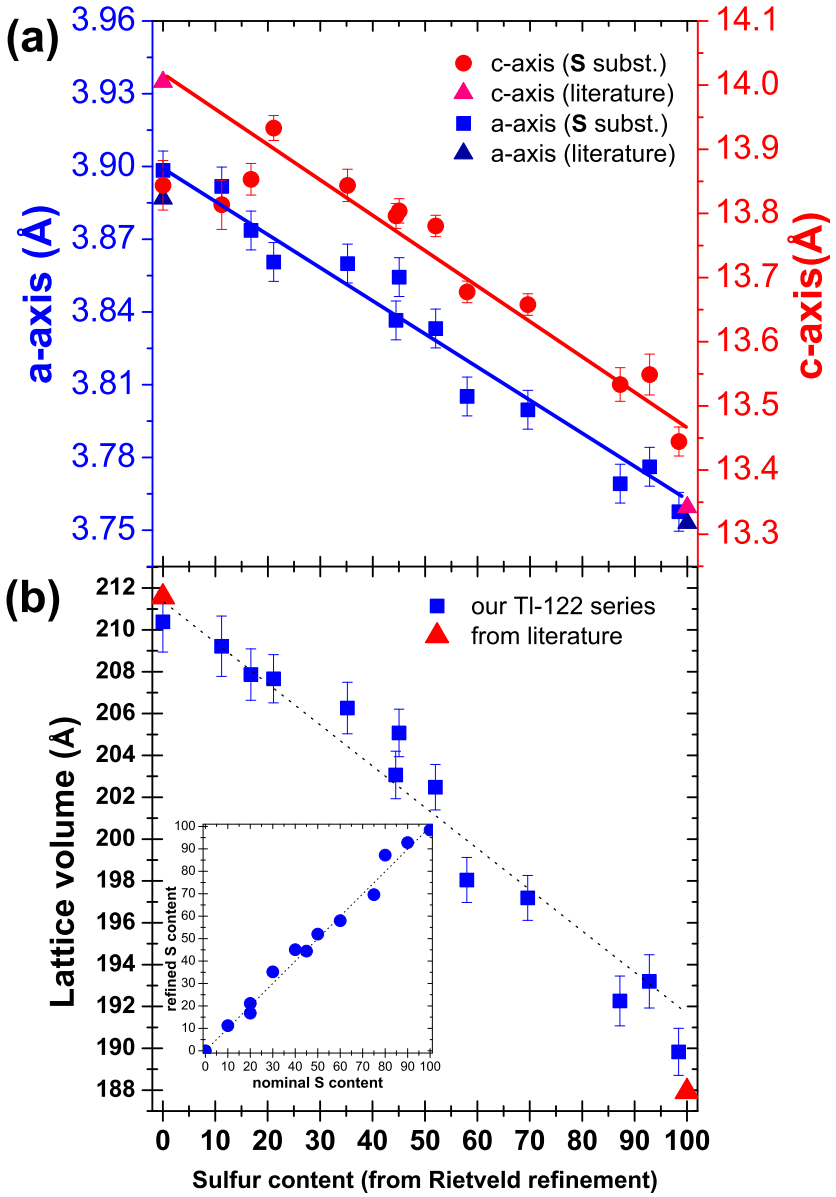

Figure 4. (a) Refined lattice parameters (from Rietveld refinement of the XRD patterns) of the $Tl_{1-y}Fe_{2-z}(Se_{1-x}S_x)_2$ samples as a function of S substitution level. Values from literature are taken from ref. [5] for the pure selenide (x=0) and ref. [19] for the pure sulfide (x=1). (b) Sulfur content dependence of the volume lattice in the $Tl_{1-y}Fe_{2-z}(Se_{1-x}S_x)_2$ samples. Inset: refined S content versus nominal S content in the series.

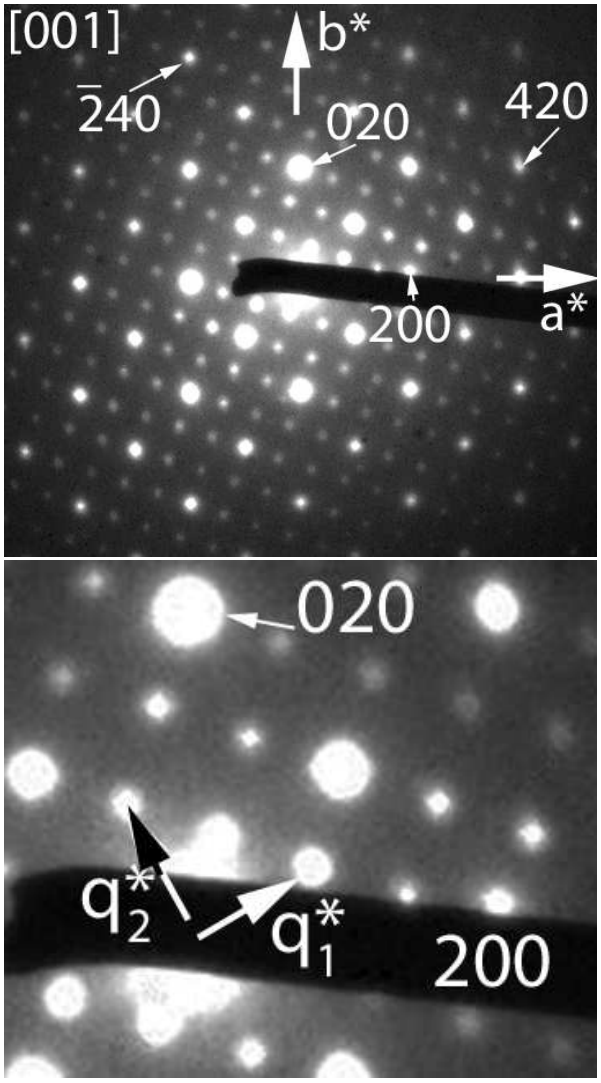

Figure 5. (Top)[001] ED pattern of x=0 sample ($Tl_{1.0(1)}Fe_{1.7(1)}Se_2$ from EDS) indexed in a tetragonal sub-cell. (Bottom) The zoomed area evidences the two directions of the modulation vector associated to the satellite reflections.

two vectors in agreement with the superstructure defined previously by Pomjakushin et al. [14] for the Cs-based 122 selenide: $\vec{q_1^*}$ and $\vec{q_2^*}$ lie along [210] and [$\bar{1}$20] directions of the subcell, with an amplitude of 1/5, leading to the values $\vec{q_1^*} = 1/10(-2\vec{a^*}+4\vec{b^*})$ and $\vec{q_2^*} = 1/10(4\vec{a^*}+2\vec{b^*})$. Bearing in mind the commensurate nature of the modulation, the structure can also be described in a supercell a = b = 8.7 Å (=$\sqrt{5}$ a), c = 14 Å (*I4/m*). This result is in agreement with neutron and x-ray powder and single crystal diffraction data reported recently on $Cs_yFe_{2-x}Se_2$ system [14] and with the electron diffraction study of $K_yFe_{2-x}Se_{\ 2}$ showing evidence of a $\sqrt{5}$ a $\times\sqrt{5}$ a $\times$ c supercell [20].

For the Se-rich composition (x = 0.2) and higher nominal iron vacancy level (z = 0.6 instead of z = 0.5 in the series, see XRD pattern, fig. 2), the EDS analysis carried out on numerous crystallites confirms a homogeneous cationic composition

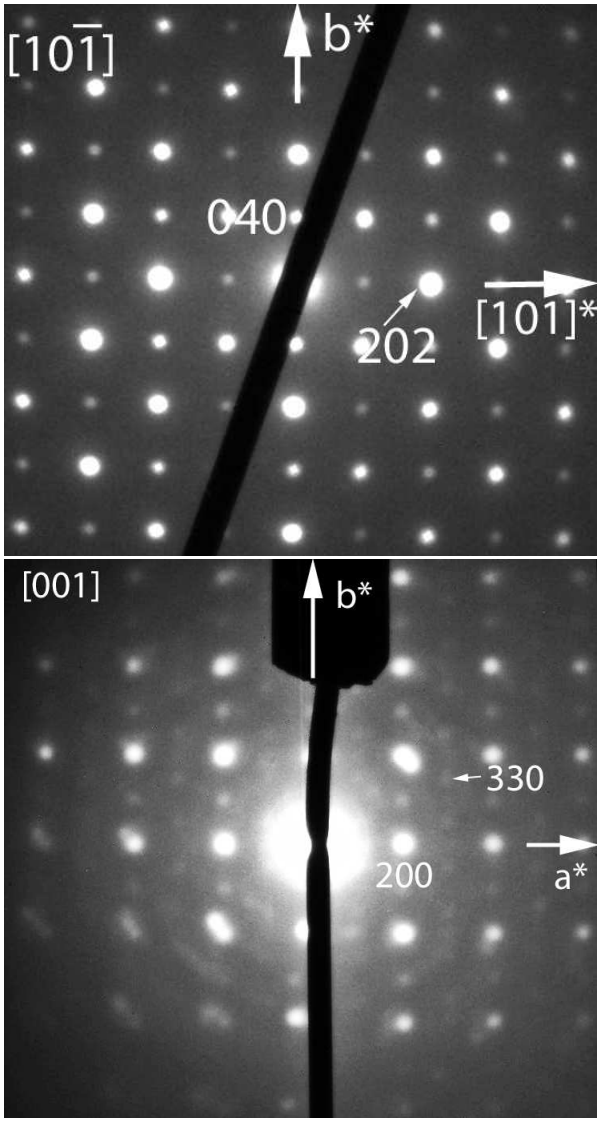

Figure 6. [10$\bar{1}$] (top) and [001] (bottom) ED pattern of x=0.2and z=0.6 sample ($Tl_{0.8(1)}Fe_{1.4(1)}(Se_{0.75(5)}S_{0.25(5)})_2$ from EDS) indexed in an orthorhombic cell.

$Tl_{0.8(1)}Fe_{1.4(1)}Se_{1.5(1)}S_{0.5(1)}$, not far from the nominal composition and with less iron than the previous sample, as expected. We note also that this sample contains a slightly lower content of thallium than the x=0 sample. The reconstruction of the reciprocal space obtained by tilting around the b* crystallographic axis led to an orthorhombic cell with the parameters a = 5.6 Å ($\sqrt{2}$ a), b = 11.3 Å (2 $\sqrt{2}$ a) and c = 15 Å (figure 6). The reflexions conditions (hkl : h+k+l=2n, 0kl : k = 2n and h0l : h = 2n) are compatible with space group *Ibam* (n ° 72). Note that the 101 and 303 reflections visible on the [10$\bar{1}$] ED pattern are artefacts caused by the multiple diffraction ; upon rotation around the [101] axis, these reflections indeed disappear depending on the zone axis. We conclude that these crystallographic features are in agreement with the indexation of extra weak peaks of the x=0.2, z=0.6 XRD pattern (see fig. 2), and also with the orthorhombic

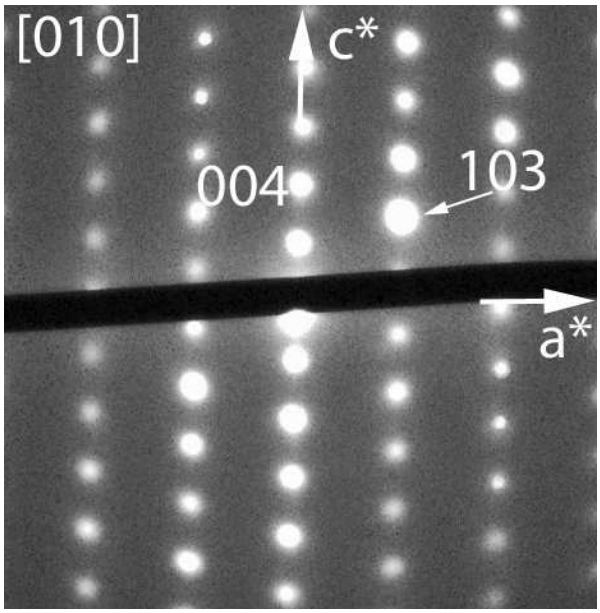

Figure 7. [010] ED pattern of x=0.7 sample ($Tl_{0.8(1)}Fe_{1.5(1)}(Se_{0.3(1)}S_{0.7(1)})_2$ from EDS) indexed in a tetragonal sub-cell.

structure obtained for the $TlFe_{1.5}S_2$ pure sulfide in 1980 [21].

For a S-rich system (x=0.7, z = 0.5) of the Tl-122(Se,S) series, a very homogeneous cationic composition close to the nominal formulation was revealed by EDS analysis. Electron diffraction evidenced the tetragonal structure as for x=0. Figure 7 exhibits an ED pattern recorded along the [010] zone axis with the parameters $a \sim 3.9$ Å and $c \sim 14$ Å.

As a conclusion, this electron diffraction study of selected x(S) compositions confirm that the extra peaks shown by x-ray diffraction (at the limit of detection level) are those due to the superstructure which appear when the iron vacancies are ordered in their basal plane. It confirms that all investigated samples of the $Tl_{0.8}Fe_{1.5}(Se_{1-x}S_x)_2$ series contain a major fraction crystallized in the iron ordered tetragonal $\sqrt{5}$ a $\times\sqrt{5}$ a $\times$ c superstructure (*I4/m*) and a minor part with the iron disordered *I4/mmm* lattice. For the sample not belonging to this series, where iron content was decreased, an orthorhombic $\sqrt{2}$ a $\times 2\sqrt{2}$ a $\times$ c superstructure was found.

3.3. Electrical resistance and magnetization

Figure 8 shows the typical magnetization curve M(T) and electrical resistance R(T) for x=0.4 sample as a function of (high) temperature. For this composition, we clearly see the onset of the antiferromagnetic (AFM) ordering around 390K on the M(T) curve. The appearance of the magnetic ordering is also visible in the R(T) curve as an anomaly which is more or less marked depending on the sulfur content. This magnetic transition (at T_N) is preceded by a structural transition (at T_S slightly above T_N) which corresponds to the ordering of iron vacancies (disordered at high T, i.e. corresponding

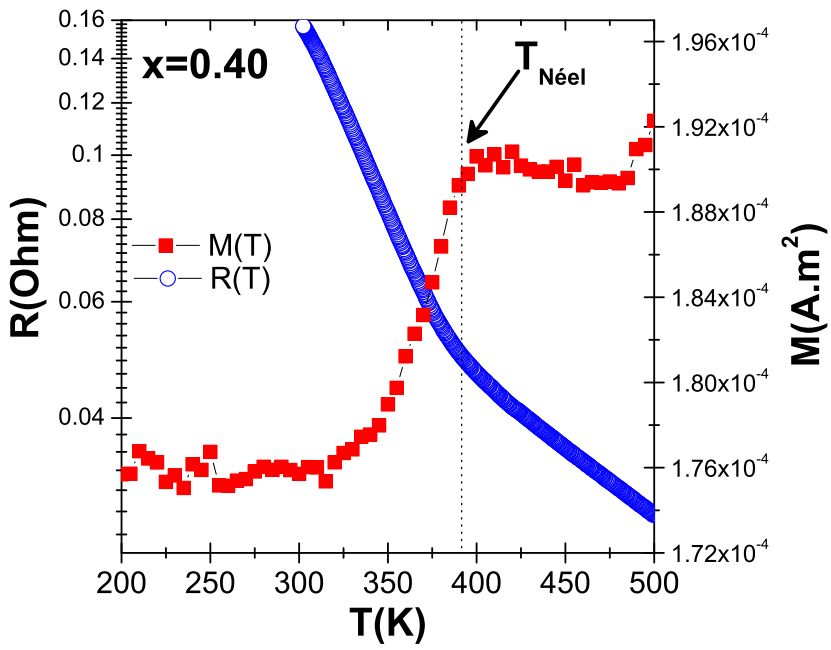

Figure 8. Magnetization measured at 6T and electrical resistance (in log scale) in the 200-500K range of the x=0.4 sample. In both measurements the signature of the onset of the AFM order at T_N is clearly visible.

to the *I4/mmm* description) in the tetragonal $\sqrt{5}$ a $\times\sqrt{5}$ a $\times$ c superstructure, as shown by our combined XRD and ED studies. A similar behavior was also reported in alkaline based selenides in previous neutron diffraction studies of $K_{0.8}Fe_{1.6}Se_2$ [6] (T_N=559K and T_S=578K) and $Rb_{0.8}Fe_{1.6}Se_2$ (T_N=502K and T_S=515K) or $Cs_{0.8}Fe_{1.6}Se_2$ (T_N=471K and T_S=500K) [16]. In thallium phases T_N and T_S seem to be very close, and we have used the anomaly in the transport measurements as a determination of T_N, as usually made in analogous alkaline-based $AFe_{2-y}Se_2$ selenides (A=K,Rb,Cs) [15, 22].

The next figure (fig. 9) shows the electrical resistance (R(T)) behaviors (in log scale) of the two extremal composition x=0 and x=1 in a larger temperature range, i.e. from 600K down to the liquid helium temperature. All compositions showed a semi-conducting behavior at low T, independently of the sulfur content. No superconductivity has been found down to 4.2K. In the particular case of the pure selenide (x=0), in the 4-300K range, the R(T) curve of our polycrystalline sample shows two regimes which intersect around T_2=120K, as observed previously by Sales et al. at 100K on a $TlFe_{1.6}Se_2$ single crystal [18]. These authors have also evidenced another transition temperature around T_1=150K, not visible in our samples, based on their specific heat, magnetization and transport measurements. And they have concluded very recently that this particular behavior of $TlFe_{1.6}Se_2$ between T_1 and T_2 was related to a sudden change of z position of 4 Fe spins pointing down (along c-axis) and 4 Fe spins pointing up in the "block checkboard" AFM structure, inducing a corrugation of the iron layer and a canting of the Fe magnetic moment relatively to the c-axis (up to 27(3) $^\circ$ at 115K)

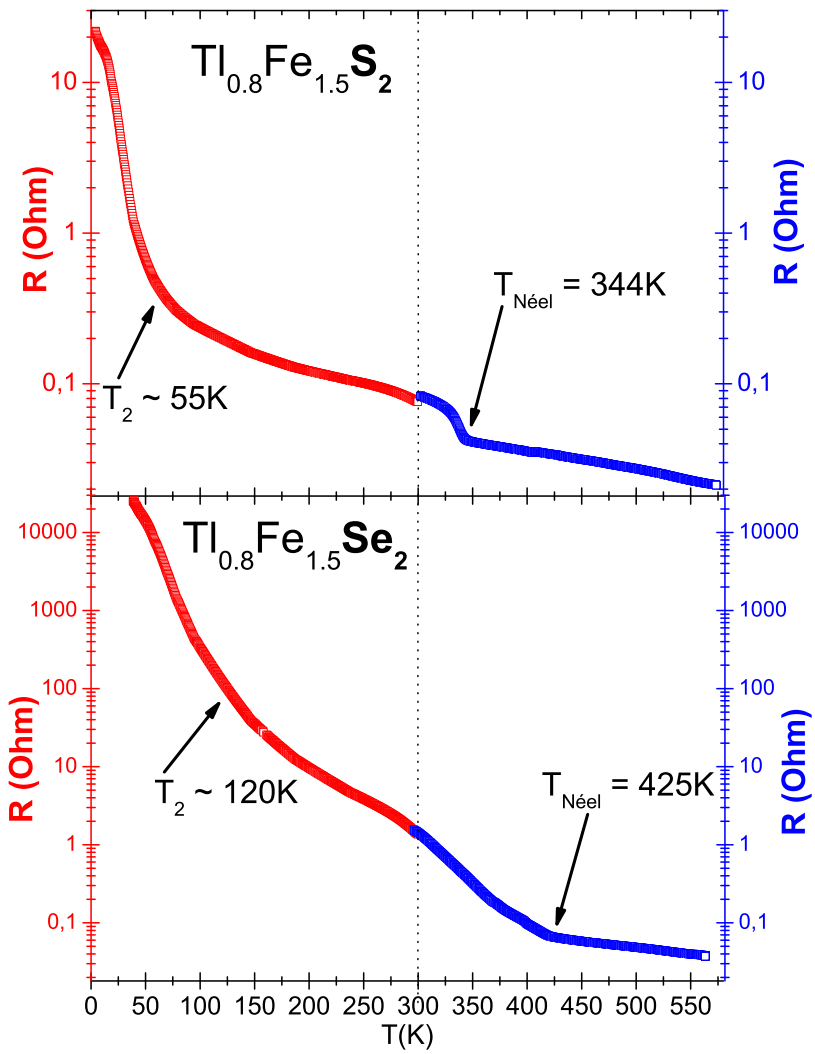

Figure 9. Low and high temperature dependence of the electrical resistance of typical x=0 and x=1.0 samples of of the $Tl_{0.8}Fe_{1.5}(Se_{1-x}S_x)_2$ series emphasizing the signature of the long range AFM structure in the ordered iron vacancies $\sqrt{5}$ a $\times\sqrt{5}$ a $\times$ c supercell at T_N.

for $T_2 < T < T_1$ [23]. We are unable with the present data to discuss in details this point, but it seems that T_2 decreases with the sulfur content introduced in the lattice. It will be maybe interesting in the future to study if this unusual magnetoelastic behavior seen in the selenide case for $T_2 < T < T_1$ persists also up to x(S)=1 and how it evolves.

The characteristic temperature T_N extracted from the anomaly observed in the high temperature resistivity measurement, and associated with the AFM ordering at low T, is clearly visible for all x(S) compositions (see curves normalized to the value measured at 573K, figure 10). It unambiguously decreases gradually in the $Tl_{0.8}Fe_{1.5}(Se_{1-x}S_x)_2$ series from T_N=425K for the selenide (x=0) to T_N=344K for the sulfide (x=1). We also note that for a fixed value of x(S), T_N can also be slightly changed by tuning the iron content

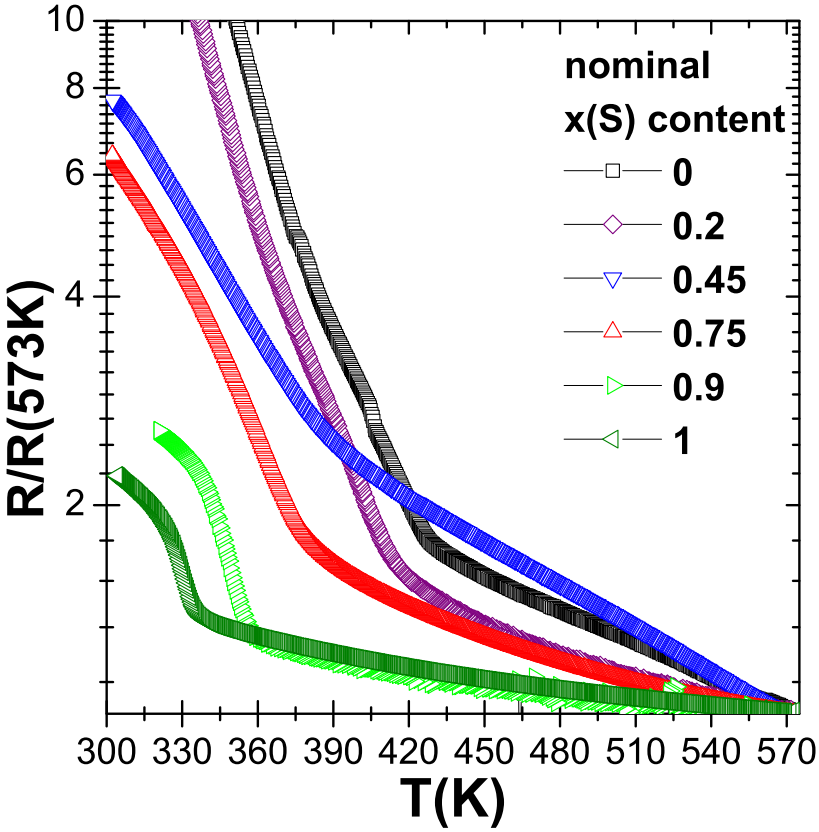

Figure 10. High temperature dependence of the electrical resistance of several $Tl_{0.8}Fe_{1.5}(Se_{1-x}S_x)_2$ samples with $0 \leq x \leq 1$. Nominal sulfur x(S) content is indicated. The anomaly related to the long range AFM structure in the ordered iron vacancies $\sqrt{5}$ a $\times\sqrt{5}$ a $\times$ c network at T_N is clearly shown and decreases with x(S).

in the lattice (i.e. the iron vacancies content), via the change of the nominal ratios Tl:Fe:Se+S (T_N is increased to 475K for example in $Tl_1Fe_{1.8}Se_2$, see its magnetization curve figure 11). However, we did not not systematically explored this trend and focused our study on the series with a nominal ratio Tl:Fe equal to 0.8:1.5. This transition from a paramagnetic state to an antiferromagnetic one at low temperature is less detectable in our magnetic measurements. This is particular true for high values of x(S), as shown in the curves of figure 11, because of a supplementary background arising from minor magnetic impurities contained in our samples (quasi undetectable by XRD). For this reason, as mentioned at the beginning of this paragraph, we have preferred the anomaly seen in the transport measurements as a determination of T_N.

3.4. Rietveld refinements in the average I4/mmm space group

The structural parameters of $Tl_{1-y}Fe_{2-z}(Se_{1-x}S_x)_2$ were refined from XRD data by the Rietveld method using the "Fullprof" software [24]. Data points with $10^\circ \leq 2\theta \leq 90^\circ$ were taken into account. A pseudo-Voigt profile shape was used. The background was

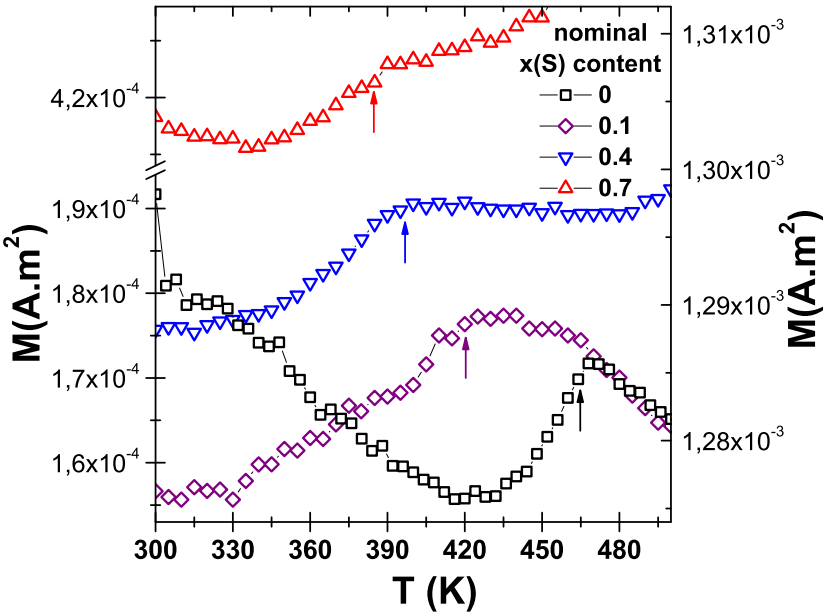

Figure 11. High temperature dependence of the magnetization (measured at 6T) of several $Tl_{1-y}Fe_{2-z}(Se_{1-x}S_x)_2$ samples for nominal x(S)=0 (and nominal composition $Tl_1Fe_{1.8}Se_2$; right scale), 0.1, 0.4 and 0.7. Nominal S/Se ratio x(S) content is indicated. The onset of the long range AFM ordering in the ordered iron vacancies network at T_N is marked by an arrow and is found to decrease with x(S).

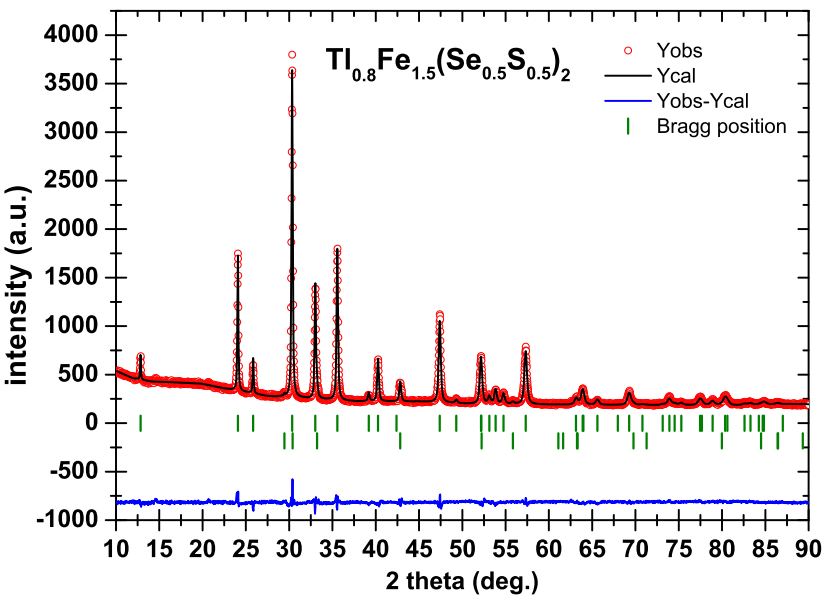

Figure 12. Rietveld refinement profile of XRD pattern (λ = 1.5406 Å) for $Tl_{0.8}Fe_{1.5}(Se_{0.5}S_{0.5})_2$ at room temperature. A difference curve is plotted at the bottom (observed minus calculated). Tick marks correspond to Bragg peaks of Tl-122(Se,S) main phase in the *I4/mmm* space group description (first line) and hexagonal Fe(Se,S) impurity phase (second line).

Table 1. Refined structural parameters of x=0, x=0.5 and x=1 compositions of $Tl_{1-y}Fe_{2-z}(Se_{1-x}S_x)_2$ series using the average *I4/mmm* description (Ch=Se,S).

compound	x=0 Häggström et al. [5] (1986)	x=0 at 250K Cao et al. [23] (2012)	x=0	x=0.5	x=1
a-axis (Å)	3.8867(3)	3.884(2)[d]	3.8870(1)	3.8331(2)	3.7572(
c-axis (Å)	14.005(1)	14.002(7)	14.0401(3)	13.781(1)	13.443(
n(Tl)	1	1	0.98(2)	0.90(2)	0.92(2
n(Fe)	1	0.795(5)[e]	0.66(2)	0.71(1)	0.70(1
n(S)	-	-	-	0.52(2)	1
z(Ch)	0.357[a]	0.3575(2)[f]	0.3530(2)	0.3541(2)	0.3478(
Fe-Ch height (Å)	1.50(1)	1.505(7)	1.446(3)	1.434(3)	1.315(5
Fe-Ch bond length (Å)	2.457(1)	2.457(2)	2.422(2)	2.394(2)	2.294(4
Ch-Fe-Ch bond angle (deg.)	104.55[b]	104.44(1)	106.70(5)	106.37(8)	110.0(1
Rp (%)	-[c]	R_1=5.89	21.3	18.0	24.7
Rwp (%)	-[c]	wRF^2=13.2	14.6	13.2	20.2
Chi^2	-[c]	8.04	3.25	0.478	4.86

[a] parameter fixed; [b] calculated; [c] not given in the paper.
[d] from neutron diffraction on single crystal in *I4/m* supercell; a-axis was divided by $\sqrt{5}$ for the comparison; [e] average value of total Fe1 (16i) and Fe2 (4d) site occupancies calculated taking into account the multiplicity of both iron sites; [f] average z-positions of Se1 (4e) and Se2 (16i) calculated taking into account the multiplicity of both selenium sites.

fitted using a linear interpolation between selected points.

Attempts to use the space group corresponding to iron vacancy ordering, for instance the tetragonal $\sqrt{5}$ a $\times$ $\sqrt{5}$ a $\times$ c lattice, led to refinement instabilities, due to the weakness of the superstructure reflections. Consequently, all refinements were carried out assuming the tetragonal *I4/mmm* lattice (space group No.139) i.e. neglecting ordering of iron vacancies.

The structure as described in the *I4/mmm* space group contains the following Wyckoff sites: Tl at 2a (0,0,0), Fe (in the center of the $FeCh_4$ tetrahedron) at 4d (0,1/2,1/4) and Ch (Ch=Se,S) at 4e (0,0,z) with z $\sim$ 0.355 (with Se and S atoms constrained to the same z coordinate). Refined variables were lattice parameters, the z-position of the chalcogen atom, iron and thallium occupancy factors and (Se,S) occupancy ratio (their total summation was constrained to unity), and all isotropic Debye Waller factors. In addition the $Fe(S_{1-x}Se_x)$ hexagonal impurity phase was taken into account in the Rietveld refinements of the XRD patterns for the samples where this minor phase was identified. Its amount and structure were refined (i.e. lattice parameters, S content (constrained to the one of the main Tl-122(Se,S) phase), profile shape parameters). For x=0.8 the Rietveld refinement was performed by taking into

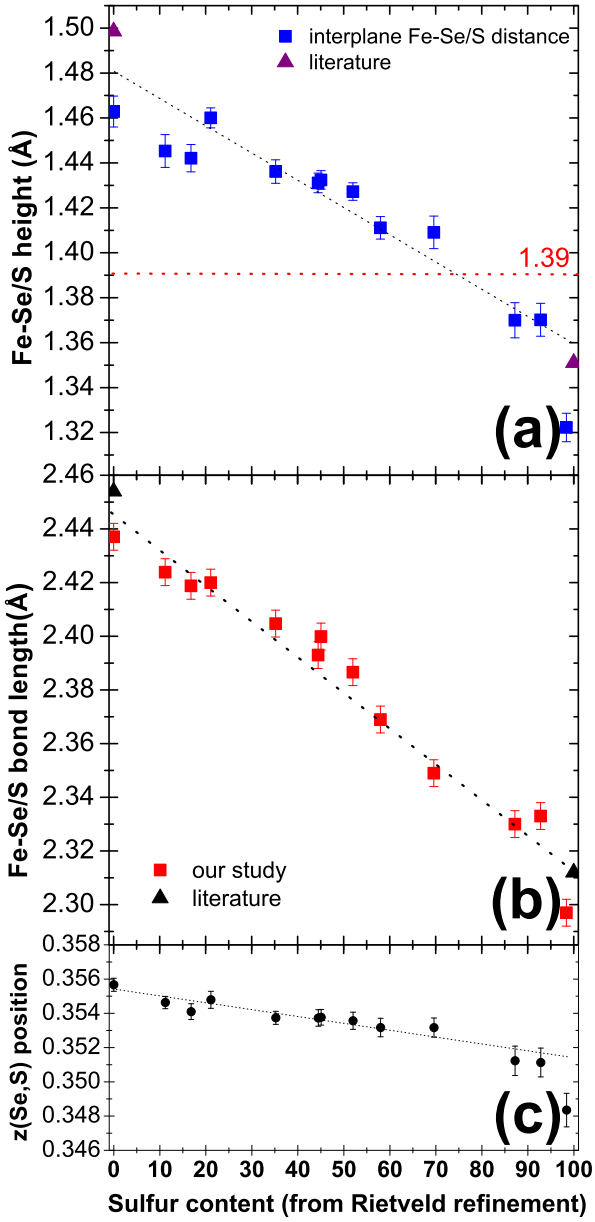

Figure 13. (a) Fe-(Se,S) height (i.e. interplane Fe-(Se,S) distance), (b) Fe-(Se,S) bond length and (c) refined z position of (Se,S) site of the $Tl_{1-y}Fe_{2-z}(Se_{1-x}S_x)_2$ samples versus the refined S content.

account the Fe_3O_4 impurity.

Figure 12 illustrates the result of the Rietveld refinement for x=0.5 as an example(see also refined values in table 1) where the minor Fe(Se,S) impurity phase was detected; there is a good agreement between the experimental and the calculated profiles. For all our samples the amount of this impurity phase was found inferior than 1% (in weight). On the other hand the refined fraction of Fe_3O_4 impurity was also found inferior than 1% (in weight) in x=0.8 sample.

Table I. gives the refined structural parameters, bond lengths and angles for x=0,

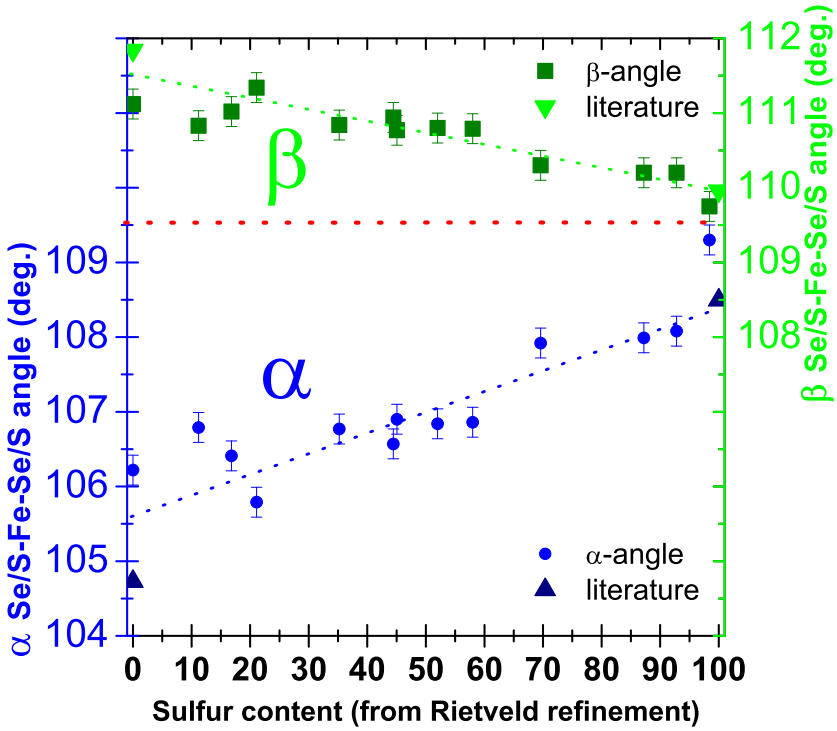

Figure 14. (Se,S)-Fe-(Se,S) bond angle in the $Fe(Se,S)_4$ tetrahedron of the $Tl_{1-y}Fe_{2-z}(Se_{1-x}S_x)_2$ samples as a function of refined S content.

x=0.5 and x=1. Our refined values for extremal $x = 0$ and $x = 1$ compositions are in good agreement with the values reported in the old (see table I) and very recent literature [5, 19, 23]. On the other hand the refined S content found in each Tl-122(Se,S) sample of the series is very close to the nominal content, as deduced from the inset of fig. 4(b). Sulfur substitutes selenium at the expected site.

Figure 13(a) shows the evolution of the Fe-(Se,S) height, i.e. the distance between the iron and the (Se,S) planes, with sulfur content. As expected the substitution of Se by S with a smaller atomic radius induces a continuous decrease of this inter-planar distance (from ~ 1.50 $\AA$ for x=0 to ~ 1.35 $\AA$ for x=1); this distance crosses the ideal value 1.39 Å for which T_c is usually maximal in pnictides [25] and the value 1.41-1.42 Å where T_c is maximal in FeSe under pressure [7]. In a similar way the Fe-(Se,S) bond length decreases regularly with sulfur content in the lattice (see fig. 13(b)) from ~ 2.45 $\AA$ in $Tl_{1-y}Fe_{2-z}Se_2$ to ~ 2.30 $\AA$ in $Tl_{1-y}Fe_{2-z}S_2$, i.e. covers the range explored under high pressure on pure tetragonal FeSe (~ 2.37 $\AA$ at 0 GPa to ~ 2.29 $\AA$ at 10 GPa) in which T_c is maximal [3, 26]. Nevertheless no superconductivity is observed in our samples down to 4.2K.

Figure 14 shows the variation of the two characteristic (Se,S)-Fe-(Se,S) bond angles in the $Fe(Se,S)_4$ tetrahedron: α and β (α notation correspond to two (Se,S) atoms of the same layer, while β notation concerns two (Se,S) atoms on both sides of the iron layer). The two complementary angles merge towards the ideal value of the regular

tetrahedron (109.47 deg.), i.e. towards the value for which the maximal T_c is observed in superconducting iron-based arsenides [8]. Again, despite this, no superconductivity is found for any (Se,S) composition.

It should be pointed out that the maximal T_c value is not achieved in FeSe iron selenide when the angle is ideal; on the contrary T_c values above 30K are reached for strongly distorted tetrahedron [3, 26].

3.5. Discussion

Rietveld refinements evidenced the continuous decrease of both Fe-(Se,S) bond length and Fe-(Se,S) height with sulfur content in $Tl_{1-y}Fe_{2-z}(Se_{1-x}S_x)_2$. As pointed out above, despite the evolution of the structural parameters towards values usually favoring superconductivity (i.e. optimal Fe-Ch height and optimal Ch-Fe-Ch angle), superconductivity is not induced by isovalent substitution of selenium by sulfur in this iron-deficient Tl-122(Se,S) system. It seems that the only way to induce bulk superconductivty in the Tl-122 system is to replace partially Tl by an alkaline element, as observed by Fang et al. for potassium substitution, with T_c around 30 K for samples rich in iron (z=0.18-0.22) [27]; they reported also superconductivity at $T_c \sim 20$ K for $Tl_1Fe_{1.7}Se_2$ composition but with a very low superconducting volume fraction, suggesting a filamentary type superconductivity associated to a minority/impurity phase.

This difference of behavior could be related to slight structural differences between pure thallium and alkaline element 122 systems. First of all, the lattice volume, and then lattice parameters, of the Tl-122 selenide are smaller than those of analogous compounds with A = K, Rb, Cs by about $1-2\%$ (see table 1 in ref [16] for a comparison). Secondly, the relative position of the chalcogen atom relatively to the iron plane in the 122 selenides remains around the same value: z=0.3530(2) in Tl-122(Se) (this work) compared to z=0.3539(2) [1]-0.3560(3) [28] in K-122 and z=0.3439(3) [28]-0.3456(4) [14] in Cs-122. This induces slightly shorter Fe-Se and Fe-Fe bond lengths in the Tl-122(Se) compared to A-122 (A = K, Rb, Cs) by $1-2\%$. These differences are enhanced when Se is substituted by S in Tl-122(Se,S) (see refined value of z(Se,S) position, fig. 13(c)), and this could affect the electronic structure, and consequently the insulating/superconducting behavior at low T.

The first DFT calculation of the electronic structure of related 122 chalcogenides was performed on stoichiometric hypothetical $TlFe_2Se_2$ and revealed that the Fermi surface is relatively close to the other iron-based compounds, i.e. contains two electron cylinders, but with hole surfaces suppressed [29]. Electronic structure calculations were then carried out on more realistic compositions: z=0.5 (with orthorhombic $\sqrt{2}$ a $\times 2\sqrt{2}$ a $\times$ c superstructure) and z=0.4 (with tetragonal $\sqrt{5}$ a $\times\sqrt{5}$ a $\times$ c supercell) and compared with alkaline-based analogous selenides [30, 31, 32]. In particular, it was found that the Fermi surface of $TlFe_{1.6}Se_2$ is in fact highly three-dimensional, unlike alkaline-based selenides [32]. Moreover, in the early calculations for z=0 (i.e. without iron vacancies), the density of states at the Fermi level $N(E_F)$ was found

to decrease from 3.6-3.94 states/(eV.cell) in Cs or K intercalated selenides [33, 34] to ca. 2 states/(eV.cell) [29] in Tl-122(Se) selenide. On the other hand, the full replacement of Se by S in K-122 was found to reduce N(E_F) by ca. 50% to 2.025 states/eV/cell for KFe_2S_2 [34]. This lower N(E_F) in the Tl-based selenide, and even lower N(E_F) with S substitution, could explain why x=0 and all S-substituted samples of the $Tl_{1-y}Fe_{2-z}(Se_{1-x}S_x)_2$ series are not superconducting at low temperature. This hypothesis has to be checked theoretically (using realistic crystallographic structures determined experimentally for the electronic structure calculations) and experimentally. In that sense ARPES measurements on pure thallium-based chalcogenides would be very useful.

Another important issue, still under debate, is the possible existence of chemical/electronic phase separation at the nanoscale in $A_{0.8}Fe_{2-z}Se_2$ selenides (A = K, Rb, Cs) suggested by TEM structural studies [20], synchrotron XRD [35] or STM studies of K-122 films [36]. Very recently, based on back-scattered electron images (SEM) and Mössbauer spectroscopy Hu. et al. suggested that superconductivity of $K_{0.8}Fe_{1.76}Se_2$ may be due to a sub-micron phase of $K_{0.6}Fe_{1.9}Se_2$ composition [37]; Texier et al. also reported a phase separation in a $Rb_{0.74}Fe_{1.6}Se_2$ single crystal studied by NMR and attributed superconductivity to the $Rb_{0.3(1)}Fe_2Se_2$ phase [38]. In the case of Tl-based 122 selenides, using Z-contrast scanning TEM, Cao et al. has reported a phase separation at the nanometer scale in crystals grown from a melt (obtained at high temperature from the mixture of pure elements) of nominal composition Tl:Fe:Se = 1:2:2 [23]. This phase separation is not due to vacancies on the thallium site but is the consequence of the incomplete ordering of iron vacancies in their $Tl_1Fe_{1.6}Se_2$ crystal (estimated to be composed of 40-48 % of ordered Fe vacancies regions). During the finalization of this manuscript, we became aware of the last report of this group who shows that fully ordered $Tl_1Fe_{1.6}Se_2$ crystals can be obtained if the composition of the melt contains less iron, typically Tl:Fe:Se = 1:1.6:2 [39]. The ratio Fe:Se we have used for the synthesis of our samples (Fe:Se = 1.5) is very close to the one used in this last report; in that sense our samples must be quite homogeneous. This is confirmed by our ED study which evidences a larger fraction of the sample crystallized in the ordered phase ($\sqrt{5}$ a $\times$ $\sqrt{5}$ a $\times$ c) than in the disorderd one ($a \times a \times c$). Indeed, contrary to A-122 selenides for which the alkaline site is strongly deficient ($y = 0.2 - 0.3$) Tl intercalated selenides can be obtained fully homogeneous, if correctly prepared, with a nearly full Tl site, i.e. $y = 0 - 0.1$ and a constant iron content distributed in fully ordered iron vacancies regions in the whole sample. Finally, all these results together imply that the doping level (then the iron valency) is very different between the actual superconducting A-122 phases and the Tl-122(Se,S) compounds, and this could also explain why superconductivity is not observed in Tl-122(Se,S).

Addressing now the high temperature magnetic behavior of the Tl-122(Se,S) series, we have plotted Néel temperature values (T_N) extracted from our transport measurements (see fig. 9 and 10) vs the sulfur content x(S) in fig. 15. It shows a regular decrease of T_N with S content. A similar trend (shifted down by 5-10K, fig.

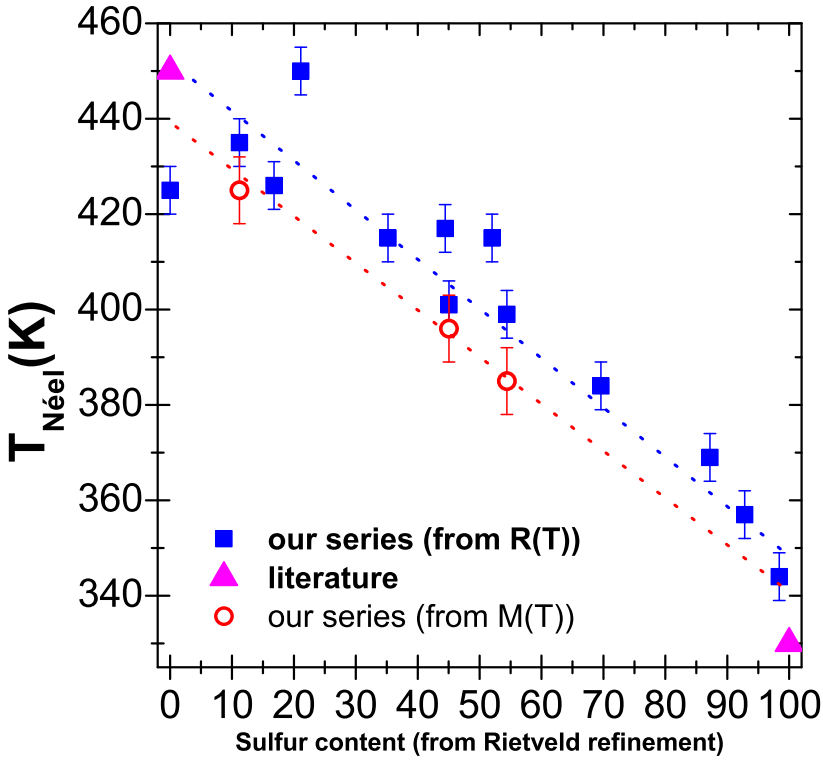

Figure 15. Néel temperature (extracted from the electrical resistance measurement) in $Tl_{1-y}Fe_{2-z}(Se_{1-x}S_x)_2$ samples versus the refined S content. The values extracted from the magnetic measurements performed on the three samples of the series (see fig. 11) have also been added.

15) is obtained considering the values extracted from the magnetic measurements of the samples (of the series) incorporating the lowest level of magnetic impurities (fig. 11). As a consequence, there is a very good correlation between T_N and the Fe-(Se,S) height (see fig. 16): T_N decreases continuously with the shrinkage of the Fe-(Se,S) height. A similar trend is observed for a plot of T_N as a function of the Fe-(Se,S) bond length (inset of fig.16).

We note that an opposite behavior has been reported in LaFeAsO when As is substituted isoelectronically by Sb: T_N decreases also monotonously with antimony substitution, corresponding to an increase of the equivalent Fe-(As,Sb) bond length [40]. This behavior results from a complex competition between different magnetic interactions in the system, i.e. the relative magnetic exchange integrals between nearest iron neighbors and next-nearest iron atoms in the same iron plane on one hand, and the magnetic exchange between iron atoms from different planes on the other. More theoretical work is necessary to interpret this linear correlation with S content, determine the different magnetic interaction energies and find the most stable magnetic configuration. The related calculations were already made for the $z = 0.4$ and $z = 0.5$ ($y = 0$ in both cases) compositions [30, 32]. It would be useful to extend it to sulfur-substituted compositions. In addition it would also be interesting to study

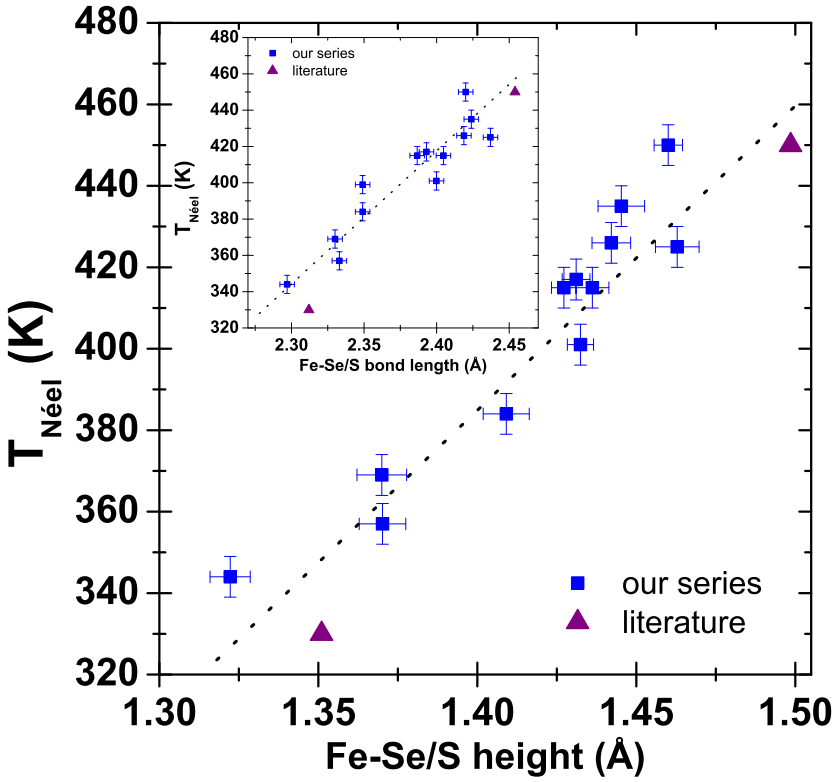

Figure 16. Néel temperature in $Tl_{1-y}Fe_{2-z}(Se_{1-x}S_x)_2$ samples (extracted from the electrical resistance measurement) as a function of the Fe-(Se,S) height in the structure. Inset: idem as a function of the Fe-(Se,S) bond length.

the evolution magnetic excitations with sulfur content in the thallium-based series and the differences with respect to their superconducting alkaline-based analogues. In view of this, we performed preliminary neutron diffraction experiments on Tl-122(Se,S) to investigate their static long-range magnetic structure. The results of this work will be published elsewhere.

4. Conclusion

The full solid solution of the $Tl_{0.8}Fe_{1.5}(Se_{1-x}S_x)_2$ series (nominal composition), i.e. from $x = 0$ to $x = 1$ was synthesized using the sealed tube technique. This sulfur-based series was carefully studied by x-ray diffraction, electron diffraction, magnetization and transport measurements. No superconductivity was found down to 4.2K despite that the optimal crystallographic parameters are reached in the S-based series, i.e. the Fe-(Se,S) height and (Se,S)-Fe-(Se,S) angle for which the critical superconducting transition T_c is usually maximal in pnictides. The S-based solid solution shows a decrease of its Néel temperature (T_N), indicating the onset of the long range antiferromagnetism in the ordered iron vacancies $\sqrt{5}$ a $\times$ $\sqrt{5}$ a $\times$ c superstructure, from 425-450K in the selenide ($x = 0$) to 330-344K in the sulfide ($x = 1$). Our structural investigation emphasizes a

direct linear relationship between T_N and the Fe-(Se,S) bond length.

Acknowledgments

The authors thank their collegues S. Karlsson, M. Núñez-Regueiro (Institut Néel) and G. Garbarino (ESRF) for their support at the first stage of this work and for their useful suggestions. We are also very grateful to André Sulpice (Institut Néel) for the low temperature magnetization measurements of tellurium substituted samples and Yves Deschanels (Institut Néel) for his help in the magnetization measurements, in particular at high temperature. This work was partially supported by the project SupraTetraFer ANR-09-BLAN-0211 of the Agence Nationale de la Recherche of France.

References

[1] J. Guo, S. Jin, G. Wang, S. Wang, K. Zhu, T. Zhou, M. He, and X. Chen. *Phy. Rev. B*, 82:180520(R), 2010.

[2] Y. Mizuguchi, F. Tomioka, S. Tsuda, T. Yamaguchi, and Y. Takano. *Appl. Phys. Lett.*, 93:152505, 2008.

[3] G. Garbarino, A. Sow, P. Lejay, A. Sulpice, P. Toulemonde, M. Mezouar, and M. Núnez-Regueiro. *Euro. Phys. Lett.*, 86:27001, 2009.

[4] S. Medvedev, T.M. McQueen, I.A. Troyan, T. Palasyuk, M. I. Eremets, R. J. Cava, S. Naghavi, F. Casper, V. Ksenofontov, G.Wortmann, and C. Felser. *Nature Materials*, 8:630, 2009.

[5] L. Häggström, H.R. Varma, B. Bjarman, R. Wäppling, and R. Berger. *J. Sol. St. Chem.*, 63:401–408, 1986.

[6] W. Bao, Q.Z. Huang, G.F. Chen, M.A. Green, D.M. Wang, J.B. He, and Y.M. Qiu. *Chin. Phys. Lett.*, 28:086104, 2011.

[7] H. Okabe, N. Takeshita, K. Horigane, T. Muranaka, and J. Akimitsu. *Phys. Rev. B*, 81:205119, 2010.

[8] C.H. Lee, A. Iyo, H. Kito, M.T. Fernandez-Diaz, T. Ito, K. Kihou, H. Mastsuhata, M. Braden, and K. Yamada. *J. Phys. Soc. Jap.*, 77:083704, 2008.

[9] H. Lei, M. Abeykoon, E.S. Bozin, K. Wang, J. B. Warren, and C. Petrovic. *Phys. Rev. Lett.*, 107:137002, 2011.

[10] D. Gu, L. Sun, Q. Wu, C. Zhang, J. Guo, P. Gao, Y. Wu, X. Dong, X. Dai, and Z. Zhao. *Phys. Rev. B*, 85:174523, 2012.

[11] T. Klein, D. Braithwaite, A. Demuer, W. Knafo, G. Lapertot, C. Marcenat, P. Rodière, I. Sheikin, P. Strobel, A. Sulpice, and P. Toulemonde. *Phys. Rev. B*, 82:184506, 2010.

[12] Y. Noat, T. Cren, V. Dubost, S. Lange, F. Debontridder, P. Toulemonde, J. Marcus, A. Sulpice, W. Sacks, and D. Roditchev. *J. Phys.: Condens. Matter*, 22:465701, 2010.

[13] H. Sabrowsky, M. Rosenberg, D. Welz, P. Deppet, and W. Schäfer. *J. Magn. Magn. Mater.*, 54-57:1497–1498, 1986.

[14] V. Yu. Pomjakushin, D. V. Sheptyakov, E. V. Pomjakushina, A. Krzton-Maziopa, K. Conder, D. Chernyshov, V. Svitlyk, and Z. Shermadini. *Phys. Rev. B*, 83:144410, 2011.

[15] Y.J. Song, Z. Wang, Z.W. Wang, H.L. Shi, Z. Chen, H.F. Tian, G.F. Chen, H.X. Yang, and J.Q. Li. *Euro. Phys. Lett*, 95:37007, 2011.

[16] F. Ye, S. Chi, W. Bao, X.F. Wang, J.J. Ying, X.H. Chen, H.D. Wang, C.H. Dong, and M. Fang. *Phys. Rev. Lett.*, 107:137003, 2011.

[17] P. Zavalij, W. Bao, X.F. Wang, J.J. Ying, X.H. Chen, D.M. Wang, J.B. He, X.Q. Wang, G.F. Chen, P.-Y. Hsieh, Q. Huang, , and M.A. Green. *Phys. Rev. B*, 83:132509, 2011.

[18] B. Sales, M.A. McGuire, A.F. May, H. Cao, B.C. Chakoumakos, and A.S. Sefat. *Phys. Rev. B*, 8:224510, 2011.

[19] K.O. Klepp and H. Boller. *Monatshefte fuer Chemie und verwandte Teile anderer Wissenschaften*, 109:1049, 1978.

[20] Z. Wang, Y. J. Song, H. L. Shi, Z. W. Wang, Z. Chen, H. F. Tian, G. F. Chen, J. G. Guo, H. X. Yang, and J. Q. Li. *Phys. Rev. B*, 83:140505(R), 2011.

[21] M. Zabel and K-J Range. *Revue de Chimie Générale*, 17:561, 1980.

[22] R. H. Liu, X. G. Luo, M. Zhang, A. F. Wang, J. J. Ying, X. F. Wang, Y. J. Yan, Z. J. Xiang, P. Cheng, G. J. Ye, Z. Y. Li, and X. H. Chen. *Euro. Phys. Lett*, 94:27008, 2011.

[23] H. Cao, C. Cantoni, A.F. May, M.A. McGuire, B.C. Chakoumakos, S.J. Pennycook, R. Custelcean, A.S. Sefat, , and Brian C. Sales. *Phys. Rev. B*, 85:054515, 2012.

[24] J. Rodriguez-Carvajal. *Physica B*, 192:55, 1993.

[25] G. Garbarino, R. Weht, A. Sow, A. Sulpice, P. Toulemonde, M. Alvarez-Murga, P. Strobel, P. Bouvier, M. Mezouar, and M. Núnez-Regueiro. *Phys. Rev. B*, 84:024510, 2011.

[26] S. Margadonna, Y. Takabayashi, Y. Ohishi, Y. Mizuguchi, Y. Takano, T. Kagayama, T. Nakagawa, M. Takata, and K. Prassides. *Phys. Rev. B*, 80:064506, 2009.

[27] M.H. Fang, H.D. Wang, C.H. Dong, Z.J. Li, C.M. Feng, J. Chen, and H.Q.Yuan. *Euro. Phys. Lett*, 94:27009, 2011.

[28] A. Krzton-Maziopa, Z. Shermadini, E. Pomjakushina, V. Pomjakushin, M. Bendele, A Amato, R. Khasanov, H. Luetkens, and K. Conder. *Journal of Physics: Condensed Matter*, 23:052203, 2011.

[29] Lijun Zhang and D. J. Singh. *Phys. Rev. B*, 79:094528, 2009.

[30] X.W. Yan, M. Gao, Z.Y. Lu, and T. Xiang. *Phys. Rev. Lett.*, 106:087005, 2011.

[31] C. Cao and J. Dai. *Phys. Rev. B*, 83:193104, 2011.

[32] C. Cao and J. Dai. *Phys. Rev. Lett.*, 107:056401, 2011.

[33] I.A. Nekrasov and M.V. Sadovskii. *JETP Letters*, 93:166, 2011.

[34] I.R. Shein and A.L. Ivanovskii. *J. Supercond. Nov. Magn.*, 24:2215, 2011.

[35] A. Ricci, N. Poccia, G. Campi, B. Joseph, G. Arrighetti, L. Barba, M. Reynolds, M. Burghammer, H. Takeya, Y. Mizuguchi, Y. Takano, M. Colapietro, N. L. Saini, and A. Bianconi. *Phys. Rev. B*, 84:060511(R), 2011.

[36] W.Li, H. Ding, P. Deng, K. Chang1, C. Song, Ke He, LiliWang, X. Ma, J.-P. Hu, Xi Chen, and Qi-K. Xue. *Nat. Phys.*, 8:126, 2012.

[37] R. Hu, E. D. Mun, D. H. Ryan, K. Cho, H. Kim, H. Hodovanets, W. E. Straszheim, M. A. Tanatar, R. Prozorov, W. N. Rowan-Weetaluktuk, J. M. Cadogan, M. M. Altarawneh, C. H. Mielke, V. S. Zapf, S. L. Bud'ko, and P. C. Canfield. *to be a chapter in the book titled "Iron Pnictide Superconductors: materials, properties and mechanism" by Pan Stanford Publishing*, page arXiv:1201.0953, 2012.

[38] Y. Texier, J. Deisenhofer, V. Tsurkan, A. Loidl, D. S. Inosov, G. Friemel, and J. Bobroff. *Phys. Rev. Lett.*, 108:237002, 2012.

[39] A. F. May, M. A. McGuire, H. Cao, I. Sergueev, C. Cantoni, B. C. Chakoumakos, D. S. Parker, , and B. C. Sales. *Phys. Rev. Lett.*, 109:077033, 2012.

[40] S. J. E. Carlsson, F. Levy-Bertrand, C. Marcenat, A. Sulpice, J. Marcus, S. Pairis, T. Klein, M. Núnez-Regueiro, G. Garbarino, T. Hansen, V. Nassif, and P. Toulemonde. *Phys. Rev. B*, 84:104523, 2011.